

Learning to Credit the Right Steps: Objective-aware Process Optimization for Visual Generation

Rui Li**

rui.li@mail.ustc.edu.cn
University of Science and Technology
of China
HeFei, China

Haibin Huang

TeleAI
ShangHai, China

Ke Hao†*

ke_hao2002@outlook.com
Shanghai Jiao Tong University
ShangHai, China

Chi Zhang

TeleAI
ShangHai, China

XueLong Li

xuelong_li@ieee.org
TeleAI
ShangHai, China

Yuanzhi Liang

TeleAI
ShangHai, China

YunGu

geron762@sjtu.edu.cn
Shanghai Jiao Tong University
ShangHai, China

Abstract

Reinforcement learning, particularly Group Relative Policy Optimization (GRPO), has emerged as an effective framework for post-training visual generative models with human preference signals. However, its effectiveness is fundamentally limited by coarse reward credit assignment. In modern visual generation, multiple reward models are often used to capture heterogeneous objectives, such as visual quality, motion consistency, and text alignment. Existing GRPO pipelines typically collapse these rewards into a single static scalar and propagate it uniformly across the entire diffusion trajectory. This design ignores the stage-specific roles of different denoising steps and produces mistimed or incompatible optimization signals. To address this issue, we propose Objective-aware Trajectory Credit Assignment (OTCA), a structured framework for fine-grained GRPO training. OTCA consists of two key components. Trajectory-Level Credit Decomposition estimates the relative importance of different denoising steps. Multi-Objective Credit Allocation adaptively weights and combines multiple reward signals throughout the denoising process. By jointly modeling temporal credit and objective-level credit, OTCA converts coarse reward supervision into a structured, timestep-aware training signal that better matches the iterative nature of diffusion-based generation. Extensive experiments show that OTCA consistently improves both image and video generation quality across evaluation metrics.

*Both authors contributed equally to this research.

†Both authors contributed equally to this research.

Permission to make digital or hard copies of all or part of this work for personal or classroom use is granted without fee provided that copies are not made or distributed for profit or commercial advantage and that copies bear this notice and the full citation on the first page. Copyrights for components of this work owned by others than the author(s) must be honored. Abstracting with credit is permitted. To copy otherwise, or republish, to post on servers or to redistribute to lists, requires prior specific permission and/or a fee. Request permissions from permissions@acm.org.
Conference acronym 'XX, Woodstock, NY

© 2018 Copyright held by the owner/author(s). Publication rights licensed to ACM.
ACM ISBN 978-1-4503-XXXX-X/2018/06
<https://doi.org/XXXXXXXX.XXXXXXX>

CCS Concepts

• **Computing methodologies** → **Computer vision tasks**.

Keywords

Reinforcement Learning, Visual Generation, Reward Signal

ACM Reference Format:

Rui Li, Ke Hao, Yuanzhi Liang, Haibin Huang, Chi Zhang, YunGu, and XueLong Li. 2018. Learning to Credit the Right Steps: Objective-aware Process Optimization for Visual Generation. In *Proceedings of Make sure to enter the correct conference title from your rights confirmation email (Conference acronym 'XX)*. ACM, New York, NY, USA, 15 pages. <https://doi.org/XXXXXXXX.XXXXXXX>

1 Introduction

Reinforcement learning (RL) is emerging as an effective paradigm for post-training visual generative models with human preference signals [6, 7, 14, 21, 24, 34]. Among existing methods, Group Relative Policy Optimization (GRPO) [10] is particularly attractive as its group-wise relative comparisons stabilize updates and improve sample quality. Recent adaptations to diffusion and flow-based generation [43, 48] further position GRPO as a promising framework for reward-driven visual alignment.

However, the effectiveness of visual GRPO is heavily shaped by the quality and design of reward supervision. Unlike supervised learning with explicit targets, GRPO improves the policy through reward-driven relative updates [26, 47]. As a result, training quality depends directly on whether the reward signal is informative, compatible, and well organized. In practice, visual generation rarely admits a single sufficient reward. Modern pipelines therefore combine multiple reward models to capture different objectives, such as visual quality, motion coherence, and text alignment[5, 29]. But these rewards are often not aligned: different reward models may favor different outputs, and naively combining them can produce conflicting optimization directions[18, 40, 45].

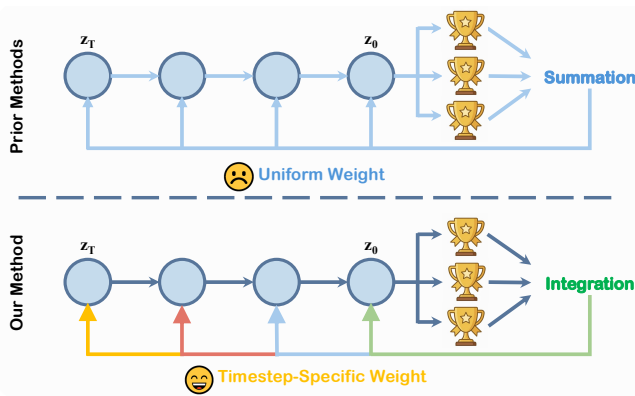


Figure 1: Comparison between our framework and existing GRPO-based approaches.

However, in GRPO-style SDE sampling, different timesteps do not contribute equally to the final output [37, 46, 49]. Existing GRPO pipelines largely ignore this heterogeneous step-wise contribution. They broadcast the same reward supervision uniformly across all timesteps, as if every generation step were equally responsible for the final outcome. This leads to misassigned policy credit: beneficial steps may be under-emphasized, while unhelpful or even detrimental steps may receive the same reinforcement, ultimately producing poorly coordinated updates along the trajectory.

We observe that the key challenge in visual GRPO is not only how to optimize, but how to organize multi-reward supervision into compatible and timestep-appropriate policy updates. To this end, we propose Objective-aware Trajectory Credit Assignment (OTCA), a structured reward credit modeling framework that performs timestep-specific credit assignment over heterogeneous reward objectives throughout the flow trajectory. OTCA combines two complementary components for temporal credit modeling and objective coordination, allowing each generation step to receive both an appropriate optimization strength and a timestep-aware objective mixture. In this way, steps more causally important to the final output receive stronger policy updates, while conflicting rewards are adaptively reconciled according to their relevance at that stage of generation. As a result, OTCA transforms multi-reward supervision from a static global signal into a structured, timestep-aware training signal. Our contributions can be summarized as follows:

- We propose **Objective-based Trajectory Credit Assignment (OTCA)**, a structured reward credit modeling framework that refines the coarse global supervision into timestep-level policy updates. OTCA jointly determines both the optimization strength and the objective mixture over heterogeneous reward signals at each timestep.
- We introduce Multi-Objective Credit Allocation (MOCA) to integrate multiple reward signals in the advantage space, avoiding optimization in the high-dimensional gradient space. We further propose Trajectory-Level Credit Decomposition (TCD) to estimate timestep-wise contribution under SDE sampling. TCD directly leverages the sampling trajectories produced by GRPO and introduces no extra modules.

- Extensive experiments show that OTCA consistently improves optimization stability and visual alignment quality, yielding superior performance across multiple metrics.

2 Related Work

RL for Visual Generation. Inspired by Proximal Policy Optimization (PPO) [32], early works [1, 6, 7] integrated reinforcement learning into diffusion models by optimizing the score function [35] with policy gradient methods, thereby enabling image generation that better aligns with human preferences. More recently, GRPO-based approaches [12, 19, 20, 27, 43, 48] have advanced visual generation to new heights. In particular, DanceGRPO [43] and FlowGRPO [48] adapt GRPO to visual generation by reformulating Flow Matching’s [21] ODE sampling into an SDE formulation, enabling online RL training on state-of-the-art generative models. VIPO [27] further enhances optimization by focusing on salient video regions through visual feature extraction, while Li et al. [20] leverage large-scale pretrained VLMs to jointly grow the generator and reward model.

Despite their success, these methods still apply a single scalar advantage uniformly across all timesteps, overlooking the heterogeneous contributions of different denoising steps. This coarse treatment ignores the nuanced information embedded in each timestep, limiting effective credit assignment in reinforcement-driven visual generation. To alleviate this issue, several recent works attempt to mitigate credit assignment ambiguity in flow-based GRPO through modified sampling strategies [8, 11, 46, 49]. Among them, G²RPO [49] explicitly identifies the sparse reward attribution problem in flow-based GRPO and introduces singular stochastic sampling. By restricting stochasticity to individual denoising steps, G²RPO seeks to provide more precise step-wise credit signals. E-GRPO [46] argues that high-entropy denoising steps drive effective exploration. It merges low-entropy steps and restricts stochastic updates to high-entropy steps to reduce reward ambiguity. While these approaches provide practical improvements, they operate by modifying how trajectories are sampled rather than changing how rewards are attributed. The supervision signal remains defined at the trajectory level, and its propagation through multi-step stochastic transitions is left intact. Consequently, the core mismatch between trajectory-level rewards and step-wise updates persists.

Reward Modeling and Multi-objective Optimization. Applying reinforcement learning to visual generation critically depends on reliable reward modeling. In image generation, preference-based models such as PickScore [16], HPSv2 [39], and ImageReward [41] estimate human visual preferences directly in pixel space. For video generation, VideoScore [13] and VideoAlign [23] extend this paradigm by evaluating visual quality, motion consistency, and text alignment, while VisionReward [40] introduces more fine-grained visual feedback signals.

Despite their effectiveness, these reward models operate on final rendered outputs and provide only global scalar supervision. They are inherently trajectory-agnostic and cannot offer timestep-level feedback within the diffusion process, where intermediate latent states determine the final outcome. In practice, post-training for visual generation typically relies on multiple reward models to jointly optimize different evaluation dimensions. This naturally formulates the problem as multi-objective optimization (MOO).

In such settings, multiple objectives may exhibit conflicting optimization directions, and fixed reward weighting fails to adaptively balance the trade-offs among them. Classical gradient-based MOO methods attempt to resolve these conflicts by explicitly operating on per-objective gradients, e.g., MGDA [4] computes a minimum-norm convex combination of task gradients, while PCGrad [44] and CAGrad [22] modify conflicting gradients to reduce interference. However, these approaches require computing and storing separate gradients for each objective at every update step, which becomes infeasible for large-scale diffusion models. To alleviate this limitation, MGDA-UB [33] derives an upper bound of the multi-objective gradient norm and proves that minimizing this bound leads to a Pareto-stationary solution under mild assumptions. By optimizing in a scaled representation space, it avoids explicit per-objective gradient computation. Another line of work addresses objective imbalance through adaptive loss reweighting methods [3], which dynamically adjust task weights based on training dynamics. However, diffusion-based alignment involves rapidly evolving objectives over limited denoising steps, rendering such dynamic estimation unreliable. More recently, Multi-GRPO [25] addresses objective imbalance in a post-training RL setting by normalizing each reward independently. This strategy primarily rescales reward magnitudes and provides limited support for true multi-objective optimization.

3 Method

We propose OTCA, a structured reward credit modeling framework for GRPO-based visual generation post-training. Our central premise is that effective policy optimization requires assigning appropriate reward signals to the right generation timesteps. To achieve this, OTCA performs joint credit assignment over timesteps and reward objectives within a unified framework, so that each generation step is assigned a credit signal that simultaneously reflects its trajectory contribution and the appropriate reward composition for optimization. Formally, the effective advantage at timestep t for sample i is defined as

$$\tilde{A}_t^i = w_t^i \cdot \sum_k c_k^i A_k^i,$$

where w_t^i reflects the relative contribution of timestep t to the final outcome, and c_k^i specifies how different reward signals should be composed at that step. Together, they define a timestep-conditioned credit signal that determines the supervision received by each denoising step, allowing policy updates to follow the actual structure of the generation trajectory rather than relying on a single global reward broadcast.

3.1 Preliminaries

GRPO for Visual Generation. The iterative denoising procedure in diffusion and flow-based models can be viewed as a sequential decision process, where each timestep corresponds to a policy action applied to the current latent state. Following [10], we adopt Group Relative Policy Optimization (GRPO) to optimize the generative policy π_θ . Given a group of G samples generated from the same prompt, GRPO maximizes the following clipped objective:

$$\mathcal{J}(\theta) = \mathbb{E}_{\{\mathbf{o}_i\} \sim \pi_{\theta_{\text{old}}}} \left[\frac{1}{G} \sum_{i=1}^G \frac{1}{T} \sum_{t=1}^T \min \left(\rho_t^i A_i, \text{clip}(\rho_t^i, 1 - \epsilon, 1 + \epsilon) A_i \right) \right], \quad (1)$$

where $\rho_t^i = \frac{\pi_\theta(\mathbf{a}_{t,i} | \mathbf{s}_{t,i})}{\pi_{\theta_{\text{old}}}(\mathbf{a}_{t,i} | \mathbf{s}_{t,i})}$ denotes the importance ratio between the current and previous policies, and $\pi_\theta(\mathbf{a}_{t,i} | \mathbf{s}_{t,i})$ is the policy probability for action $\mathbf{a}_{t,i}$ at state $\mathbf{s}_{t,i}$.

The advantage A_i is computed using group-wise normalized rewards:

$$A_i = \frac{r_i - \text{mean}(r_1, r_2, \dots, r_G)}{\text{std}(r_1, r_2, \dots, r_G)}. \quad (2)$$

This normalization measures the relative performance of each sample within the group and stabilizes policy optimization.

Stochastic Sampling for Flow Models. Flow-matching models typically define generation through a deterministic ordinary differential equation (ODE),

$$dz_t = \mathbf{u}_t dt, \quad (3)$$

where \mathbf{u}_t denotes the learned velocity field. While this formulation is effective for generation, its deterministic nature produces only a single trajectory for each initialization, which limits the trajectory diversity required by policy optimization methods such as GRPO.

To introduce exploration, we follow prior work and consider a reverse-time stochastic differential equation (SDE),

$$dz_t = \left(\mathbf{u}_t - \frac{1}{2} \epsilon_t^2 \nabla_{z_t} \log p_t(z_t) \right) dt + \epsilon_t dw, \quad (4)$$

where ϵ_t controls the noise magnitude and dw is standard Brownian motion. Compared with the deterministic ODE, this SDE induces stochastic trajectory sampling and thus enables exploration over multiple denoising paths. The score function can be written in closed form as

$$\nabla_{z_t} \log p_t(z_t) = -\frac{z_t - \alpha_t \mathbf{x}}{\sigma_t^2}. \quad (5)$$

Substituting this score into the reverse-time SDE yields a stochastic sampling process that can be naturally interpreted as a policy $\pi_\theta(\mathbf{a}_t | \mathbf{s}_t)$, making flow-based generation compatible with GRPO-style reinforcement learning.

3.2 Trajectory-Level Credit Decomposition

In GRPO, the trajectory-level advantage A_i is uniformly broadcast to all timesteps, implicitly treating each denoising step as equally credit-worthy. This assumption can be overly coarse for diffusion-based generation, where different timesteps may contribute unevenly to the final outcome. The issue can become more pronounced under SDE sampling [36], where stochastic exploration introduces additional variability into the denoising trajectory. As a result, some intermediate transitions may provide clearer evidence of useful progress, while others may be less informative or temporarily less aligned with the eventual denoised result. Assigning the same policy signal to all such steps can therefore introduce unnecessary variance into optimization and yield unreliable updates.

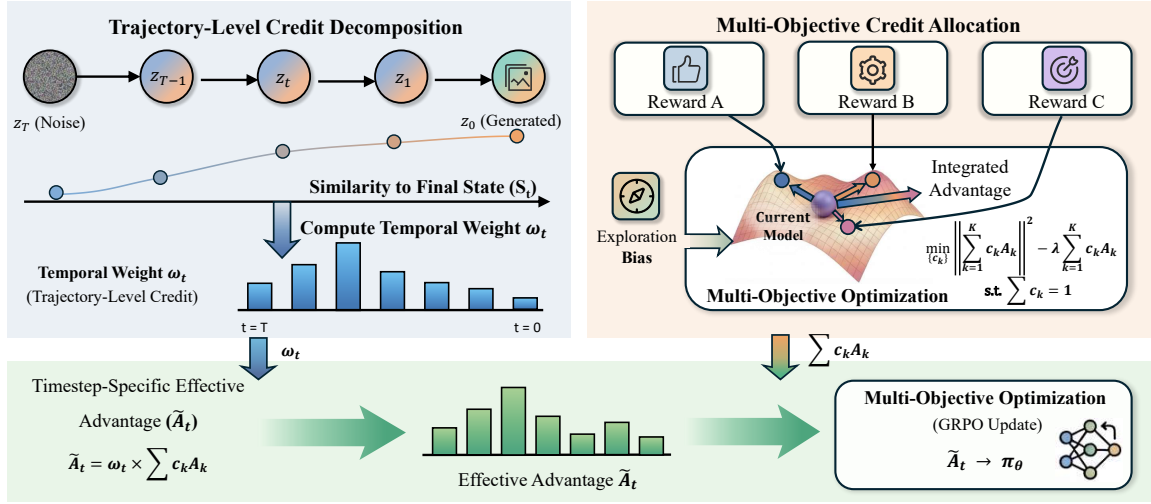


Figure 2: Overview of our method. Different from existing GRPO-based approaches, our pipeline explicitly injects multiple objective optimization signals into each temporal timestep dimension, enabling balanced optimization at the timestep level.

To make policy optimization more sensitive to the denoising trajectory, we introduce a temporal credit assignment mechanism that estimates the relative importance of each timestep. Inspired by prior work that uses cosine similarity as a scale-invariant measure of representation alignment [2, 9], we quantify how well each intermediate latent state aligns with the final denoised latent state [28]. Let z_t^i denote the latent representation of the i -th sample at timestep t , and let z_{final}^i denote the corresponding final denoised latent representation. We define the cosine similarity between them as

$$S_t^i = \frac{z_t^i \cdot z_{\text{final}}^i}{\|z_t^i\| \|z_{\text{final}}^i\|}. \quad (6)$$

Here, S_t^i serves as a practical proxy for timestep-wise alignment toward the terminal denoised state. Rather than relying on the absolute similarity value itself, we focus on how this alignment changes across consecutive timesteps, since a larger increase in similarity indicates that the corresponding transition makes a stronger relative contribution toward the final denoised outcome. Specifically, we compute the similarity difference between consecutive timesteps:

$$\Delta S_t^i = S_t^i - S_{t+1}^i. \quad (7)$$

A larger ΔS_t^i indicates that timestep t is associated with a larger increase in alignment toward the final denoised state, and is therefore treated as more important in the trajectory.

To maintain stability and compatibility with GRPO, we convert these step-wise alignment changes into normalized non-negative temporal weights:

$$w_t^i = \frac{\max(0, \Delta S_t^i) + \epsilon}{\sum_{\tau} (\max(0, \Delta S_{\tau}^i) + \epsilon)}, \quad (8)$$

where ϵ is a small constant used to avoid degenerate zero weights. These weights redistribute the trajectory-level advantage across timesteps according to their relative contribution, allowing GRPO to place stronger policy updates on more informative denoising steps

instead of uniformly broadcasting the same optimization signal throughout the trajectory.

3.3 Multi-Objective Credit Allocation

Temporal credit assignment identifies which denoising steps deserve stronger policy updates, but effective supervision in visual generation also depends on how reward signals are composed at those steps. In practice, policy optimization is driven by multiple heterogeneous objectives, such as visual quality, motion quality, and text alignment, whose interactions can be nontrivial and whose relevance may vary across the denoising trajectory. However, existing GRPO methods typically reduce these objectives to a single scalar reward and apply the resulting supervision uniformly during optimization. This fixed reward composition is often too coarse to reflect the evolving needs of generation, motivating an adaptive objective credit mechanism that assigns step-conditioned reward weights throughout the trajectory.

Advantage-Space Multi-Objective Fusion. To address this, we formulate the balancing of competing rewards as a Multi-Objective Optimization (MOO) problem. Traditional gradient-based MOO seeks a conflict-aware, Pareto-stationary update direction by solving a minimum-norm problem:

$$\min_{\{c_k\}_{k=1}^K} \left\| \sum_{k=1}^K c_k \nabla_{\theta} \mathcal{L}_k(\theta) \right\|^2 \quad \text{s.t.} \quad \sum_{k=1}^K c_k = 1, \quad c_k \geq 0 \quad \forall k, \quad (9)$$

where c_k is the dynamic weight assigned to the k -th objective, and $\nabla_{\theta} \mathcal{L}_k(\theta)$ is the corresponding gradient. However, computing and storing per-objective gradients for modern large-scale generative models is computationally prohibitive, making this direct approach infeasible for online RL. Inspired by MGDA-UB [33], which proves that optimizing an upper bound of the multi-objective gradient norm yields a Pareto-stationary solution, we bypass this bottleneck by projecting the optimization from the gradient space into the advantage space. Using the chain rule from the policy gradient

theorem, the gradient norm can be bounded as follows:

$$\begin{aligned} \left\| \sum_{k=1}^K c_k \nabla_{\theta} \mathcal{L}_k(\theta) \right\|_2^2 &= \left\| \sum_{k=1}^K c_k \nabla_{\theta} \left(\frac{\pi_{\theta}}{\pi_{\theta_{\text{old}}}} A_k \right) \right\|_2^2 \\ &= \left\| \sum_{k=1}^K c_k \frac{1}{\pi_{\theta_{\text{old}}}} A_k \nabla_{\theta} \pi_{\theta} \right\|_2^2 \\ &\leq \left\| \sum_{k=1}^K c_k A_k \right\|_2^2 \left\| \frac{1}{\pi_{\theta_{\text{old}}}} \nabla_{\theta} \pi_{\theta} \right\|_2^2. \end{aligned} \quad (10)$$

Since the policy gradient term $\frac{1}{\pi_{\theta_{\text{old}}}} \nabla_{\theta} \pi_{\theta}$ is shared across objectives for a fixed sample i during a given update step, the per-objective gradients differ only by their scalar advantages A_k^i . Under this shared-direction structure, the gradient-space multi-objective optimization problem can be reformulated as a low-dimensional optimization over scalar advantages:

$$\min_{\{c_k^i\}_{k=1}^K} \left\| \sum_{k=1}^K c_k^i A_k^i \right\|_2^2 \quad \text{s.t.} \quad \sum_{k=1}^K c_k^i = 1, \quad c_k^i \geq 0 \quad \forall k, \quad (11)$$

where A_k^i is the group-wise normalized advantage of sample i for the k -th objective.

Adaptive Exploration Mechanism. However, a naive application of this minimum-norm solver introduces a new challenge: **overly conservative policy updates**. Because the solver strictly penalizes variance among competing objectives, it naturally favors "safe", compromised directions where all advantages are small but equal. This cautious behavior discourages the policy from taking bold steps toward high-reward but conflicting directions, potentially trapping the generative model in mediocre local optima. To break this conservative deadlock and ensure robust policy discovery, we introduce a dynamic exploration mechanism. We first quantify an exploration signal e_i based on the structural deviation of the trajectory from the group average:

$$q_i = \sum_{t=1}^T w_t^i \cdot \Delta S_t^i, \quad e_i = \frac{|q_i|}{\text{std}(\{q_j\}_{j=1}^G) + \epsilon}, \quad (12)$$

where G is the group size. A high e_i indicates that the generation path is highly distinctive, signaling a valuable region for exploration. We then inject an exploration bias into the objective-level solver:

$$\min_{\{c_k^i\}} \left\| \sum_{k=1}^K c_k^i A_k^i \right\|_2^2 - \lambda_i \sum_{k=1}^K c_k^i A_k^i \quad \text{s.t.} \quad \sum_{k=1}^K c_k^i = 1, \quad c_k^i \geq 0 \quad \forall k, \quad (13)$$

where the added penalty term encourages the solver to maximize the total weighted advantage rather than strictly minimizing the norm. To prevent unstable divergence, the exploration strength λ_i is dynamically modulated:

$$\lambda_i = \frac{\max\left(0, \sum_{k=1}^K A_k^i\right)}{\left|\sum_{k=1}^K A_k^i\right| + \epsilon} \cdot \tanh(e_i). \quad (14)$$

Under this formulation, exploration emerges only when the aggregated advantage is positive and the trajectory exhibits significant structural deviation. With the temporal weights w_t^i and the adaptive objective coefficients c_k^i , the final effective advantage at timestep t

is defined as

$$\tilde{A}_t^i = w_t^i \sum_{k=1}^K c_k^i A_k^i.$$

This effective advantage provides a unified training signal for visual GRPO: it redistributes policy credit across denoising steps according to their relative contribution, while adaptively composing multiple reward signals during optimization. As a result, policy updates become better matched to the structure of the generation trajectory, yielding more stable optimization and improved generation quality.

3.4 Optimization Target

Finally, we incorporate the proposed credit assignment scheme into the GRPO objective by replacing the original trajectory-level advantage A_i in Eq. 1 with the timestep-specific effective advantage \tilde{A}_t^i . The resulting policy objective is defined as:

$$\begin{aligned} \mathcal{J}_{\text{OTCA}}(\theta) &= \mathbb{E}_{\substack{\{o_i\}_{i=1}^G \sim \pi_{\theta_{\text{old}}}(\cdot|c) \\ a_{t,i} \sim \pi_{\theta_{\text{old}}}(\cdot|s_{t,i})}} \left[\frac{1}{G} \sum_{i=1}^G \frac{1}{T} \sum_{t=1}^T \right. \\ &\quad \left. \min \left(\rho_t^i \tilde{A}_t^i, \text{clip}(\rho_t^i, 1 - \epsilon, 1 + \epsilon) \tilde{A}_t^i \right) \right]. \end{aligned} \quad (15)$$

By combining timestep-sensitive weighting with adaptive reward composition into a single effective advantage, OTCA provides a unified training signal for visual GRPO. This effective advantage allows policy updates to concentrate on more informative denoising steps while adapting the reward composition to the evolving needs of the generation trajectory.

As a result, OTCA makes reinforcement learning updates better aligned with the multi-stage nature of visual generation. Rather than uniformly broadcasting a coarse global reward across the entire trajectory, the resulting policy signal is redistributed according to step-wise contribution and reward relevance, leading to more stable optimization and improved generation quality.

4 Experiment

4.1 Settings

Datasets. Both image and Video generation are finetuned with the prompts from DanceGRPO, which contains 50k prompts spanning various styles. We randomly separate 1K data as our test set for image generation.

Backbones and Rewards. For image generation, we fine-tune FLUX.1-dev [17] using three reward models: CLIP-T [30], HPSv2.1 [39], and the LAION aesthetic predictor [31]. We assess generalization on both in-domain and out-of-domain benchmarks including PickScore [16] and ImageReward [42]. For video generation, we fine-tune Wan2.2-T2V-14B-480P [38] with VideoAlign, which provides reward signals along three dimensions: visual quality, motion quality, and text alignment. For out-of-domain evaluation on video generation, we adopt VBench [15], which evaluates video quality across multiple dimensions.

Implementation Details. For image generation, we set the group size to $G = 12$, downsample training resolution to 512×512 , and use 16 sampling steps. For video generation, we set the group size to $G = 32$, training resolution to $240 \times 416 \times 53$ ($H \times W \times T$), and use 16 sampling steps to accelerate training. During inference, we

Table 1: Comparison of different methods on image-level reward metrics.

Method	CLIP-T \uparrow	Aesthetic \uparrow	HPS \uparrow	PickScore \uparrow	ImageReward \uparrow
Flux	0.2682	6.2508	0.2986	22.66	1.1001
DanceGRPO	0.2619	6.8917	0.3018	22.70	1.0172
VIPO	0.2722	6.7813	0.3026	22.69	1.1128
Ours	0.3071	6.6028	0.3225	22.97	1.1998

increase the resolution to 512×512 with 50 inference steps for Flux, and $480 \times 832 \times 53$ with 50 inference steps for Wan2.2-T2V-14B. All image generation experiments are conducted on 8 NVIDIA H100 GPUs, while video generation experiments are trained on 32 NVIDIA H100 GPUs. The stochasticity parameter η is set to 0.3 for Flux and 0.8 for Wan2.2, with a learning rate of 1×10^{-5} and 5×10^{-6} respectively. Additional hyperparameter details are provided in the supplementary material.

4.2 Quantitative Results

4.2.1 Image Generation Quantitative Results. We evaluate OTCA on FLUX.1-dev and compare it against the base FLUX model, DanceGRPO, and VIPO. We first report the in-domain metrics used during training, including CLIP-T, LAION-Aesthetic, and HPSv2.1. To further assess whether the improvements extend beyond the training reward distribution, we additionally evaluate out-of-domain generalization using PickScore and ImageReward.

As shown in Table 1, OTCA outperforms the base model and prior GRPO-based variants on most evaluation metrics. It achieves the strongest results on preference-oriented measures, including CLIP-T, HPS, PickScore, and ImageReward. The improvements are consistent across both in-domain and out-of-domain evaluations, indicating better generalization beyond the training rewards.

In contrast, DanceGRPO and VIPO show less balanced performance. For instance, while DanceGRPO yields competitive aesthetic scores, it experiences noticeable degradation on semantic-oriented metrics. This discrepancy indicates a common limitation of uniform reward broadcasting: the policy tends to disproportionately favor aesthetic quality at the expense of semantic fidelity. OTCA effectively mitigates this optimization bias via adaptive multi-objective allocation, yielding a more favorable trade-off across diverse preference dimensions, as reflected by the consistent gains in CLIP-T and PickScore. Similarly, although VIPO generally improves upon the base model, it consistently underperforms OTCA across key preference measures. These results suggest that simply combining multiple rewards is insufficient for stable alignment.

Overall, the results show that reorganizing reward supervision along the generation trajectory leads to more balanced optimization. By coordinating credit assignment across timesteps and objectives, OTCA better captures multi-dimensional human preferences.

4.2.2 Video Generation Quantitative Results. To evaluate the effectiveness of OTCA on video generation, we conduct comprehensive quantitative evaluations on VBench, a comprehensive benchmark suite for video generative models. We adopt DanceGRPO [?] as the baseline, representing one of the most recent and widely adopted

GRPO-based methods for visual generation. Table 3 presents the VBench results across overall evaluation metrics.

As shown in Table 2, OTCA achieves consistent improvements over both the original Wan2.2 model and DanceGRPO across the majority of evaluation dimensions. Our method demonstrates significant gains in Dynamic Degree, indicating enhanced motion fidelity and more natural temporal dynamics. The improvement in Spatial Relationship suggests that OTCA better preserves spatial coherence and object interactions across frames. Furthermore, Multiple Objects shows substantial improvement, reflecting the ability to handle complex scenes with multiple entities. The gains in Color demonstrate that OTCA not only improves motion quality but also enhances visual fidelity. The improvements in Scene understanding and Subject Consistency further confirm that our dual credit assignment mechanism enables more effective alignment with both semantic and stylistic preferences.

Notably, while VideoAlign provides separate rewards for Visual Quality, Motion Quality, and Text Alignment, the timestep-level supervision offered by OTCA automatically balances these objectives according to the generation stage. The improvements in semantic-related dimensions such as Scene and Spatial Relationship emerge as a natural consequence of this trajectory credit optimization, as timesteps contribute more receive stronger supervision signals that guide global composition and semantic structure. Additionally, OTCA delivers clear gains on the overall VBench benchmark, achieving better Quality Score, Semantic Score, and Total Score than the baseline.

For video generation, OTCA enables finer-grained guidance for policy updates by effectively balancing multiple reward models, making it a strong new baseline for post-training video generation.

We attribute these improvements to two complementary factors. First, OTCA adaptively coordinates multiple reward signals, reducing the interference that often arises among heterogeneous reward models. This is particularly important when the reward models are relatively coarse, since naively combining them can easily introduce unstable or conflicting optimization signals. The issue is even more pronounced in video generation, where videos sampled under SDE-based exploration are often of relatively low quality during training, while current video reward models remain less precise and robust than their image counterparts. In such cases, effective coordination across reward signals becomes especially important for stabilizing optimization. Second, OTCA redistributes supervision across denoising timesteps instead of broadcasting a uniform optimization signal throughout the trajectory. This is especially important for GRPO-style policy optimization, where different timesteps contribute unequally to the final outcome. Together, these two mechanisms make reward optimization both more compatible across objectives and more precise along the diffusion trajectory, leading to more stable and effective training.

4.3 Qualitative Experiment

4.3.1 Image Generation Qualitative Results. As shown in Fig. 3, OTCA consistently produces more faithful and visually appealing images than the baselines. For human-related prompts, it generates more coherent layouts, richer details, and stronger realism, while for object-centric prompts, it yields more vivid anthropomorphic effects

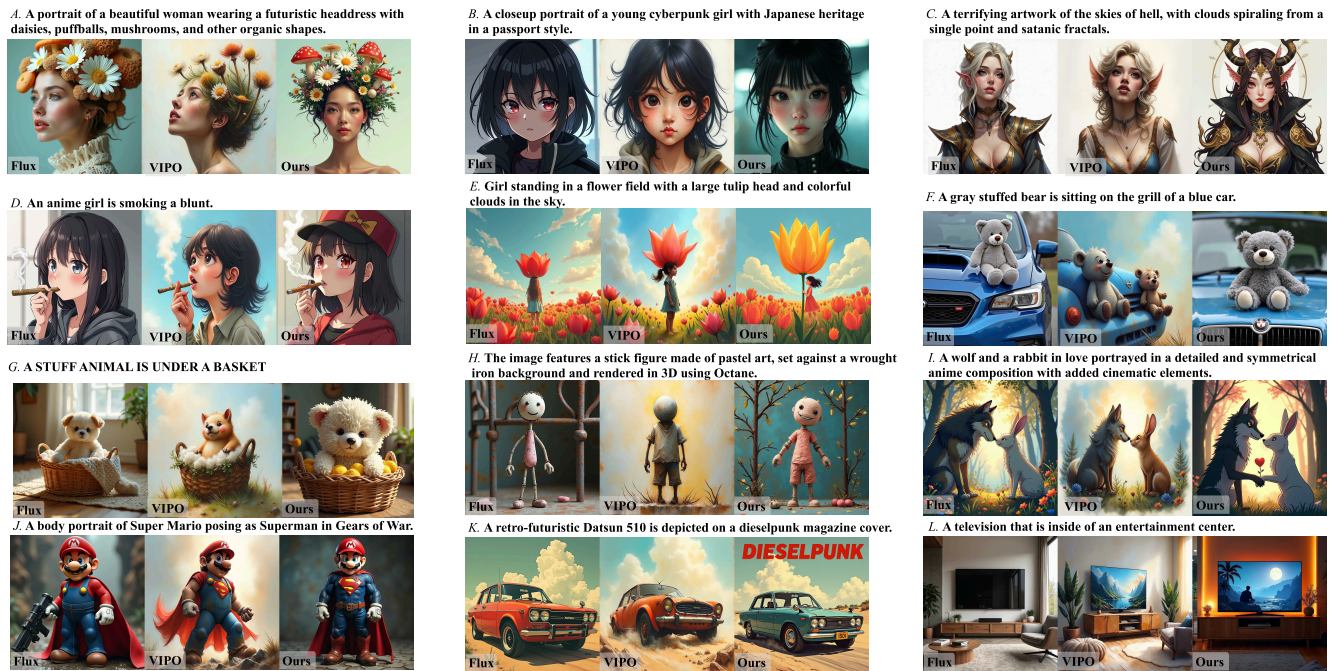


Figure 3: Qualitative comparison on image generation. Our method produces images with higher fidelity and aesthetic quality compared to existing GRPO-based approaches, demonstrating clearer structures and more consistent temporal alignment.

Table 2: Quantitative comparison on the VBench benchmark. OTCA consistently outperforms other methods across key dimensions.

Method	Color	Dynamic Degree	Imaging Quality	Multiple Objects	Scene	Spatial Relation	Subject Consistency
Wan2.2	89.79	70.83	68.34	63.79	35.90	80.54	93.78
DanceGRPO	90.35	71.45	67.93	64.85	35.18	83.25	93.76
OTCA (Ours)	92.88	75.00	68.58	68.45	38.45	88.57	93.95

Table 3: Overall VBench scores comparison. OTCA achieves consistent improvements across quality, semantic, and total scores.

Method	Quality Score	Semantic Score	Total Score
Wan2.2	83.30	73.10	81.26
DanceGRPO	83.31	73.31	81.31
Ours	83.72	75.19	82.01

and more diverse visual expressions. In challenging cases like case H and I, OTCA also better captures the intended interactions and preserves semantic consistency, whereas even the strong baseline VIPO may degrade, likely due to its limited coordination across multiple reward signals and the lack of fine-grained timestep-level credit assignment.

4.3.2 Video Generation Qualitative Results. As shown in Fig. 4, in Case A, both Wan2.2 and DanceGRPO generate dragon breath that spreads across the entire frame, which is physically implausible.

Table 4: Ablation study on image-level reward metrics. Best results are highlighted in bold.

Ablation	CLIP-T ↑	Aesthetic ↑	HPS ↑	PickScore ↑	ImageReward ↑
Flux	0.2682	6.2508	0.2986	22.66	1.1001
MOCA-only	0.2787	6.2120	0.3049	22.64	1.1250
TCD-only	0.2708	6.3270	0.3104	22.87	1.2618
Ours (Full)	0.3071	6.6028	0.3225	22.97	1.1998

In contrast, our method produces a more realistic and properly localized breath effect. In Case B, neither Wan nor DanceGRPO correctly captures the process in which a sheet of paper is folded into a dragon. Our method successfully renders this transformation while also achieving more visually appealing results. In Case C, our method produces more accurate and realistic liquid dynamics.

These qualitative examples provide further evidence for the effectiveness of OTCA. Overall, OTCA generates videos with better physical plausibility, more faithful motion evolution, and stronger semantic consistency. We attribute these advantages to its process-aware optimization: by adaptively coordinating heterogeneous reward signals and redistributing supervision across denoising timesteps, OTCA provides more effective guidance for visual generation.

4.4 Ablation Studies

4.4.1 Reward Metric Results. We conduct an ablation study on image-level reward metrics to disentangle the effect of OTCA’s key components. Table 4 reports the results of two simplified variants, *TCD-Only* and *MOCA-Only*, together with the full model.

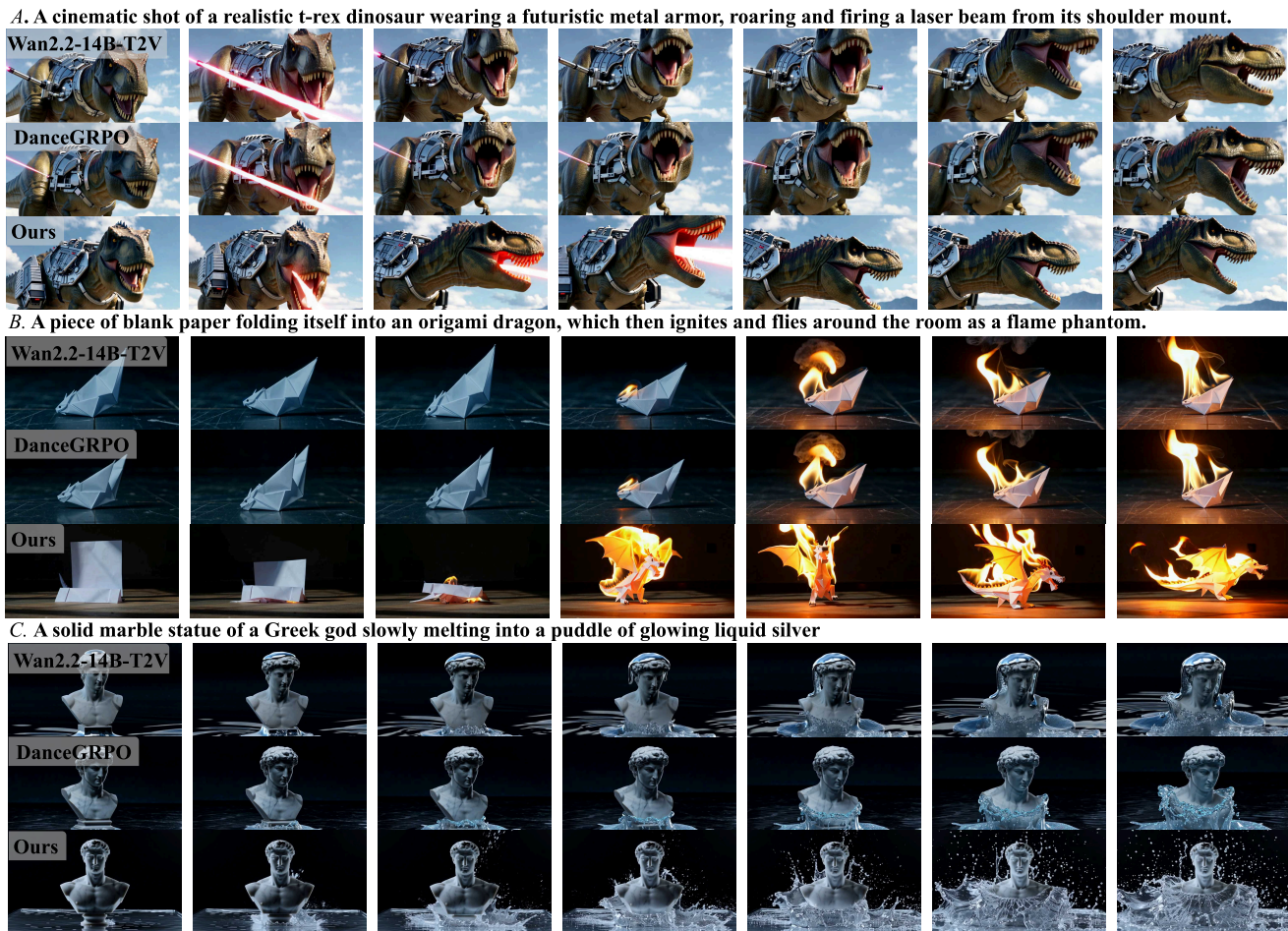


Figure 4: Qualitative comparison on video generation. From top to bottom: results generated by Wan2.2 (baseline), DanceGRPO, and our proposed OTCA. Our method produces more detailed and perceptually pleasing results, with richer textures, more accurate colors, and better semantic alignment to the prompt.

Compared with the base FLUX model, both *TimeStep-Only* and *Reward Integration-Only* improve overall performance, confirming that each component contributes positively to the final generation quality. Specifically, *TCD-Only* improves CLIP-T and HPS over the baseline, suggesting that trajectory-level credit decomposition helps allocate supervision more effectively across the denoising trajectory. However, its improvement in aesthetic quality remains limited, suggesting that temporal credit assignment alone is insufficient to fully capture high-level preference signals without integrating multiple reward signals.

In contrast, *MOCA-Only* achieves the better HPS and ImageReward scores, showing that direct reward fusion is effective for strengthening alignment with reward-oriented objectives. Nevertheless, its improvements on CLIP-T, Aesthetic, and PickScore are still weaker than those of the full model, implying that reward integration alone may bias optimization toward a subset of reward signals without fully improving holistic perceptual quality.

Our full model achieves the best results on CLIP-T, HPS and PickScore, while remaining second best on ImageReward, demonstrating the complementary nature of the two components. These results suggest that timestep-aware credit assignment and reward integration address different aspects of the optimization problem: the former improves where supervision should be emphasized, while the latter improves what should be optimized. Their combination yields a more balanced and effective optimization strategy, leading to consistently stronger overall performance.

4.4.2 Reward Curve Results. To further examine the contribution of different design choices, we present the reward curves of all variants throughout training. As shown in the figure 5, the full model converges faster and achieves higher final reward values across all three metrics than the simplified variants. Using only the latent credit assign or only the reward signal integration already yields clear improvements over the baseline, while their combination delivers the strongest overall performance, indicating that the two signals provide complementary supervision. Moreover, compared

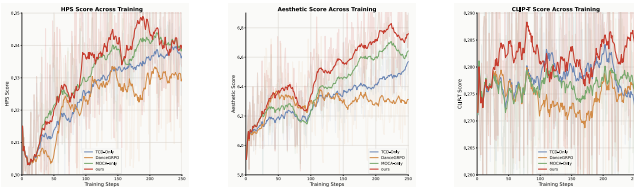


Figure 5: Reward curves on different ablation during training.

with DanceGRPO, our method exhibits a more stable upward trend during training, suggesting that OTCA provides more reliable and effective optimization signals.

5 Conclusion

In this paper, we present OTCA, a structured reward credit modeling framework for GRPO-based visual generation. Our key insight is that reinforcement learning for diffusion and flow-based generation should not rely on a single global reward uniformly broadcast across the entire denoising trajectory. Instead, effective optimization requires answering two coupled questions: which timesteps deserve stronger policy supervision, and which reward objectives should dominate at each stage of generation. To this end, OTCA introduces a unified credit assignment mechanism that jointly models timestep importance and adaptive multi-objective fusion, transforming coarse trajectory-level supervision into fine-grained, process-aware policy updates. Extensive experiments on both image and video generation demonstrate that OTCA consistently improves visual quality, semantic alignment, and optimization stability over strong GRPO-based baselines. Ablation studies further verify that temporal credit assignment and adaptive reward integration contribute complementary benefits. Overall, our results suggest that structured reward credit modeling is a promising direction for scaling reinforcement learning in visual generation, and we hope OTCA can serve as a useful step toward more precise and reliable post-training of generative models.

References

- [1] Kevin Black, Michael Janner, Yilun Du, Ilya Kostrikov, and Sergey Levine. 2023. Training diffusion models with reinforcement learning. *arXiv preprint arXiv:2305.13301* (2023).
- [2] Ting Chen, Simon Kornblith, Mohammad Norouzi, and Geoffrey Hinton. 2020. A simple framework for contrastive learning of visual representations. In *International conference on machine learning*. PmlR, 1597–1607.
- [3] Zhao Chen, Vijay Badrinarayanan, Chen-Yu Lee, and Andrew Rabinovich. 2018. GradNorm: Gradient normalization for adaptive loss balancing in deep multitask networks. In *International conference on machine learning*. PMLR, 794–803.
- [4] Jean-Antoine Désidéri. 2012. Multiple-gradient descent algorithm (MGDA) for multiobjective optimization. *Comptes Rendus. Mathématique* 350, 5-6 (2012), 313–318.
- [5] Nicolas Dufour, Lucas Degeorge, Arijit Ghosh, Vicky Kalogeiton, and David Picard. 2025. MIRO: Multi-Reward cOnditioned pretraining improves T2I quality and efficiency. *arXiv preprint arXiv:2510.25897* (2025).
- [6] Ying Fan and Kangwook Lee. 2023. Optimizing ddpn sampling with shortcut fine-tuning. *arXiv preprint arXiv:2301.13362* (2023).
- [7] Ying Fan, Olivia Watkins, Yuqing Du, Hao Liu, Moonkyung Ryu, Craig Boutilier, Pieter Abbeel, Mohammad Ghavamzadeh, Kangwook Lee, and Kimin Lee. 2023. Dpok: Reinforcement learning for fine-tuning text-to-image diffusion models. *Advances in Neural Information Processing Systems* 36 (2023), 79858–79885.
- [8] Shiran Ge, Chenyi Huang, Yuang Ai, Qihang Fan, Huaibo Huang, and Ran He. 2025. Expand and Prune: Maximizing Trajectory Diversity for Effective GRPO in Generative Models. *arXiv preprint arXiv:2512.15347* (2025).
- [9] Jean-Bastien Grill, Florian Strub, Florent Altché, Corentin Tallec, Pierre Richemond, Elena Buchatskaya, Carl Doersch, Bernardo Avila Pires, Zhaohan Guo, Mohammad Gheshlaghi Azar, et al. 2020. Bootstrapping your own latent-a new approach to self-supervised learning. *Advances in neural information processing systems* 33 (2020), 21271–21284.
- [10] Daya Guo, Dejian Yang, Haowei Zhang, Junxiao Song, Ruoyu Zhang, Runxin Xu, Qihao Zhu, Shirong Ma, Peiyi Wang, Xiao Bi, et al. 2025. Deepseek-r1: Incentivizing reasoning capability in llms via reinforcement learning. *arXiv preprint arXiv:2501.12948* (2025).
- [11] Dailan He, Guanlin Feng, Xingtong Ge, Yazhe Niu, Yi Zhang, Bingqi Ma, Guanglu Song, Yu Liu, and Hongsheng Li. 2025. Neighbor GRPO: Contrastive ODE Policy Optimization Aligns Flow Models. *arXiv preprint arXiv:2511.16955* (2025).
- [12] Xiaoxuan He, Siming Fu, Yuke Zhao, Wanli Li, Jian Yang, Dacheng Yin, Fengyun Rao, and Bo Zhang. 2025. Tempflow-grpo: When timing matters for grpo in flow models. *arXiv preprint arXiv:2508.04324* (2025).
- [13] Xuan He, Dongfu Jiang, Ge Zhang, Max Ku, Achint Soni, Sherman Siu, Haonan Chen, Abhramil Chandra, Ziyang Jiang, Aaran Arulraj, et al. 2024. Videoscore: Building automatic metrics to simulate fine-grained human feedback for video generation. *arXiv preprint arXiv:2406.15252* (2024).
- [14] Jonathan Ho, Ajay Jain, and Pieter Abbeel. 2020. Denoising diffusion probabilistic models. *Advances in neural information processing systems* 33 (2020), 6840–6851.
- [15] Ziqi Huang, Yanan He, Jiashuo Yu, Fan Zhang, Chenyang Si, Yuming Jiang, Yuanhan Zhang, Tianxing Wu, Qingyang Jin, Nattapol Chanpaisit, et al. 2024. Vbench: Comprehensive benchmark suite for video generative models. In *Proceedings of the IEEE/CVF Conference on Computer Vision and Pattern Recognition*. 21807–21818.
- [16] Yuval Kirstain, Adam Polyak, Uriel Singer, Shahbuland Matiana, Joe Penna, and Omer Levy. 2023. Pick-a-pic: An open dataset of user preferences for text-to-image generation. *Advances in neural information processing systems* 36 (2023), 36652–36663.
- [17] Black Forest Labs. 2024. Flux. <https://github.com/black-forest-labs/flux>.
- [18] Kyungmin Lee, Xiaohong Li, Qifei Wang, Junfeng He, Junjie Ke, Ming-Hsuan Yang, Irfan Essa, Jinwoo Shin, Feng Yang, and Yinxiao Li. 2025. Calibrated multi-preference optimization for aligning diffusion models. In *Proceedings of the Computer Vision and Pattern Recognition Conference*. 18465–18475.
- [19] Junzhe Li, Yutao Cui, Tao Huang, Yiping Ma, Chun Fan, Miles Yang, and Zhao Zhong. 2025. Mixgrpo: Unlocking flow-based grpo efficiency with mixed ode-sde. *arXiv preprint arXiv:2507.21802* (2025).
- [20] Rui Li, Yuanzhi Liang, Ziqi Ni, Haibing Huang, Chi Zhang, and Xuelong Li. 2025. Growing with the Generator: Self-paced GRPO for Video Generation. *arXiv preprint arXiv:2511.19356* (2025).
- [21] Yaron Lipman, Ricky TQ Chen, Heli Ben-Hamu, Maximilian Nickel, and Matt Le. 2022. Flow matching for generative modeling. *arXiv preprint arXiv:2210.02747* (2022).
- [22] Bo Liu, Xingchao Liu, Xiaojie Jin, Peter Stone, and Qiang Liu. 2021. Conflict-averse gradient descent for multi-task learning. *Advances in neural information processing systems* 34 (2021), 18878–18890.
- [23] Jie Liu, Gongye Liu, Jiajun Liang, Ziyang Yuan, Xiaokun Liu, Mingwu Zheng, Xiele Wu, Qiulin Wang, Wenyu Qin, Menghan Xia, et al. 2025. Improving video generation with human feedback. *arXiv preprint arXiv:2501.13918* (2025).
- [24] Xingchao Liu, Chengyue Gong, and Qiang Liu. 2022. Flow straight and fast: Learning to generate and transfer data with rectified flow. *arXiv preprint arXiv:2209.03003* (2022).
- [25] Qiang Lyu, Zicong Chen, Chongxiao Wang, Haolin Shi, Shibo Gao, Ran Piao, Youwei Zeng, Jianlou Si, Fei Ding, Jing Li, et al. 2025. Multi-GRPO: Multi-Group Advantage Estimation for Text-to-Image Generation with Tree-Based Trajectories and Multiple Rewards. *arXiv preprint arXiv:2512.00743* (2025).
- [26] Weijia Mao, Hao Chen, Zhenheng Yang, and Mike Zheng Shou. 2025. The Image as Its Own Reward: Reinforcement Learning with Adversarial Reward for Image Generation. *arXiv preprint arXiv:2511.20256* (2025).
- [27] Ziqi Ni, Yuanzhi Liang, Rui Li, Yi Zhou, Haibing Huang, Chi Zhang, and Xuelong Li. 2025. Seeing What Matters: Visual Preference Policy Optimization for Visual Generation. *arXiv preprint arXiv:2511.18719* (2025).
- [28] Ziqi Pang, Xin Xu, and Yu-Xiong Wang. 2025. Aligning generative denoising with discriminative objectives unleashes diffusion for visual perception. *arXiv preprint arXiv:2504.11457* (2025).
- [29] Mihir Prabhudesai, Russell Mendonca, Zheyang Qin, Katerina Fragkiadaki, and Deepak Pathak. 2024. Video diffusion alignment via reward gradients. *arXiv preprint arXiv:2407.08737* (2024).
- [30] Alec Radford, Jong Wook Kim, Chris Hallacy, Aditya Ramesh, Gabriel Goh, Sandhini Agarwal, Girish Sastry, Amanda Askell, Pamela Mishkin, Jack Clark, et al. 2021. Learning transferable visual models from natural language supervision. In *International conference on machine learning*. PmlR, 8748–8763.
- [31] Christoph Schuhmann, Romain Beaumont, Richard Vencu, Cade Gordon, Ross Wightman, Mehdi Cherti, Theo Coombes, Aarush Katta, Clayton Mullis, Mitchell Wortsman, et al. 2022. Laion-5b: An open large-scale dataset for training next generation image-text models. *Advances in neural information processing systems* 35 (2022), 25278–25294.

- [32] John Schulman, Filip Wolski, Prafulla Dhariwal, Alec Radford, and Oleg Klimov. 2017. Proximal policy optimization algorithms. *arXiv preprint arXiv:1707.06347* (2017).
- [33] Ozan Sener and Vladlen Koltun. 2018. Multi-task learning as multi-objective optimization. *Advances in neural information processing systems* 31 (2018).
- [34] Jiaming Song, Chenlin Meng, and Stefano Ermon. 2020. Denoising diffusion implicit models. *arXiv preprint arXiv:2010.02502* (2020).
- [35] Yang Song, Jascha Sohl-Dickstein, Diederik P Kingma, Abhishek Kumar, Stefano Ermon, and Ben Poole. 2020. Score-based generative modeling through stochastic differential equations. *arXiv preprint arXiv:2011.13456* (2020).
- [36] Yang Song, Jascha Sohl-Dickstein, Diederik P Kingma, Abhishek Kumar, Stefano Ermon, and Ben Poole. 2020. Score-based generative modeling through stochastic differential equations. *arXiv preprint arXiv:2011.13456* (2020).
- [37] Thuy Phuong Vu, Mai Viet Hoang Do, Minhhuu Le, Dinh-Cuong Hoang, and Phan Xuan Tan. 2026. Memorization Control in Diffusion Models from Denoising-centric Perspective. *arXiv preprint arXiv:2601.21348* (2026).
- [38] Team Wan, Ang Wang, Baole Ai, Bin Wen, Chaojie Mao, Chen-Wei Xie, Di Chen, Feiwu Yu, Haiming Zhao, Jianxiao Yang, et al. 2025. Wan: Open and advanced large-scale video generative models. *arXiv preprint arXiv:2503.20314* (2025).
- [39] Xiaoshi Wu, Yiming Hao, Keqiang Sun, Yixiong Chen, Feng Zhu, Rui Zhao, and Hongsheng Li. 2023. Human preference score v2: A solid benchmark for evaluating human preferences of text-to-image synthesis. *arXiv preprint arXiv:2306.09341* (2023).
- [40] Jiazheng Xu, Yu Huang, Jiale Cheng, Yuanming Yang, Jiajun Xu, Yuan Wang, Wenbo Duan, Shen Yang, Qunlin Jin, Shurun Li, et al. 2024. Visionreward: Fine-grained multi-dimensional human preference learning for image and video generation. *arXiv preprint arXiv:2412.21059* (2024).
- [41] Jiazheng Xu, Xiao Liu, Yuchen Wu, Yuxuan Tong, Qinkai Li, Ming Ding, Jie Tang, and Yuxiao Dong. 2023. Imagereward: Learning and evaluating human preferences for text-to-image generation. *Advances in Neural Information Processing Systems* 36 (2023), 15903–15935.
- [42] Jiazheng Xu, Xiao Liu, Yuchen Wu, Yuxuan Tong, Qinkai Li, Ming Ding, Jie Tang, and Yuxiao Dong. 2023. ImageReward: Learning and Evaluating Human Preferences for Text-to-Image Generation. In *NeurIPS*.
- [43] Zeyue Xue, Jie Wu, Yu Gao, Fangyuan Kong, Lingting Zhu, Mengzhao Chen, Zhiheng Liu, Wei Liu, Qiushan Guo, Weilin Huang, et al. 2025. DanceGRPO: Unleashing GRPO on Visual Generation. *arXiv preprint arXiv:2505.07818* (2025).
- [44] Tianhe Yu, Saurabh Kumar, Abhishek Gupta, Sergey Levine, Karol Hausman, and Chelsea Finn. 2020. Gradient surgery for multi-task learning. *Advances in neural information processing systems* 33 (2020), 5824–5836.
- [45] Sixian Zhang, Bohan Wang, Junqiang Wu, Yan Li, Tingting Gao, Di Zhang, and Zhongyuan Wang. 2024. Learning multi-dimensional human preference for text-to-image generation. In *Proceedings of the IEEE/CVF Conference on Computer Vision and Pattern Recognition*. 8018–8027.
- [46] Shengjun Zhang, Zhang Zhang, Chensheng Dai, and Yueqi Duan. 2026. E-GRPO: High Entropy Steps Drive Effective Reinforcement Learning for Flow Models. *arXiv preprint arXiv:2601.00423* (2026).
- [47] Mingzhe Zheng, Weijie Kong, Yue Wu, Dengyang Jiang, Yue Ma, Xuanhua He, Bin Lin, Kaixiong Gong, Zhao Zhong, Liefeng Bo, et al. 2026. Manifold-Aware Exploration for Reinforcement Learning in Video Generation. *arXiv preprint arXiv:2603.21872* (2026).
- [48] Da Zhou, Yang Li, Qing Li, Yujia Yang, Jian Tang, Yelong Shen, Xiang Li, Xinyang Wang, and Pan Zhou. 2024. Flow-GRPO: Training Flow Matching Models via Online Reinforcement Learning. In *Proceedings of the International Conference on Learning Representations (ICLR)*. <https://arxiv.org/abs/2312.06699>
- [49] Yujie Zhou, Pengyang Ling, Jiayi Bu, Yibin Wang, Yuhang Zang, Jiaqi Wang, Li Niu, and Guangtao Zhai. 2025. G2rpo: Granular grpo for precise reward in flow models. *arXiv preprint arXiv:2510.01982* 3 (2025).

6 Appendix

6.1 Timestep Contribution Proxy

A key assumption of our method is that ΔS_t^i serves as a reliable proxy for the contribution of each denoising timestep. To examine this assumption, we decode the intermediate latent state Z_t^i at each timestep t along the sampling trajectory and compare ΔS_t^i with the corresponding reward improvement ΔR_t^i . Intuitively, if ΔS_t^i faithfully captures timestep-wise contribution to the final generation outcome, then timesteps with larger ΔS_t^i should also be associated with larger reward gains, respectively larger contribution.

Quantitative evidence. Table 5 summarizes the quantitative relationship between ΔS_t^i and ΔR_t^i over 511 sampled trajectories.

Table 5: Correlation analysis between ΔS_t^i and ΔR_t^i . The results support the use of ΔS_t^i as a proxy for timestep contribution.

Metric	Range	Value
Pearson correlation \uparrow	$[-1, 1]$	0.9091 ± 0.028
Spearman correlation \uparrow	$[-1, 1]$	0.8381 ± 0.077
Pairwise order agreement \uparrow	$[0, 1]$	0.8428 ± 0.049
Recall@3 \uparrow	$[0, 1]$	0.770
Recall@5 \uparrow	$[0, 1]$	0.892
Argmax distance \downarrow	$[0, 15]$	0.74

First, we examine their global correlation by analysing the correlation coefficient. The results indicates that ΔS_t^i exhibits a strong positive linear association with ΔR_t^i . In detail, the Pearson correlation achieves 0.909, highly correlated. This indicates that timesteps with larger latent similarity increase tend to gain larger reward improvements. The same trend also exists at the ranking level, the Spearman correlation reaches 0.838, suggesting that ΔS_t^i remains highly consistent with ΔR_t^i in capturing the relative importance of different denoising steps.

Beyond global correlation, we further assess whether ΔS_t^i can accurately localize the timesteps that contribute most to reward improvement. The pairwise order agreement, which measures the fraction of timestep pairs whose relative ordering is consistent between ΔS_t^i and the true reward change ΔR_t^i , reaches 0.842. This shows that the ranking induced by ΔS_t^i closely matches that of ΔR_t^i . In addition, the average argmax distance between the peaks of ΔS_t^i and ΔR_t^i is only 0.74 steps in the total 16 sampling steps, indicating that the most salient timestep identified by ΔS_t^i is typically very close to the true reward-critical step. This localization ability is further supported by the substantial overlap between the high-response regions, with Recall@3 = 0.770 and Recall@5 = 0.892.

Overall, these results consistently support the use of ΔS_t^i as an effective proxy for timestep contribution. These metrics provide empirical justification for using ΔS_t^i to allocate fine-grained optimization strength across denoising steps.

Qualitative evidence. To further provide intuitive evidence for the validity of ΔS_t^i as a proxy for timestep contribution, we visualize the relationship between ΔS_t^i and ΔR_t^i along the sampling trajectory for several representative examples in Fig. 6. As shown, the two signals exhibit highly consistent temporal patterns across different cases. Timesteps with larger ΔS_t^i generally coincide with more pronounced reward improvements, while low-response steps tend to yield only limited reward gains. This suggests that ΔS_t^i captures the relative contribution of each timestep to the final quality improvement.

Moreover, as shown in Fig. 6, in most illustrated cases the timestep with the largest ΔS_t^i tends to yield the greatest reward gain ΔR_t^i . Even when not perfectly aligned, the deviation is typically limited to only 1–2 neighboring timesteps and still falls within the same high-response region. The above qualitative experiments further demonstrate the reliability of using timestep increase as an indicator of each timestep contribution.

Overall, these qualitative observations are highly consistent with the quantitative findings. From an intuitive perspective, ΔS_t^i closely

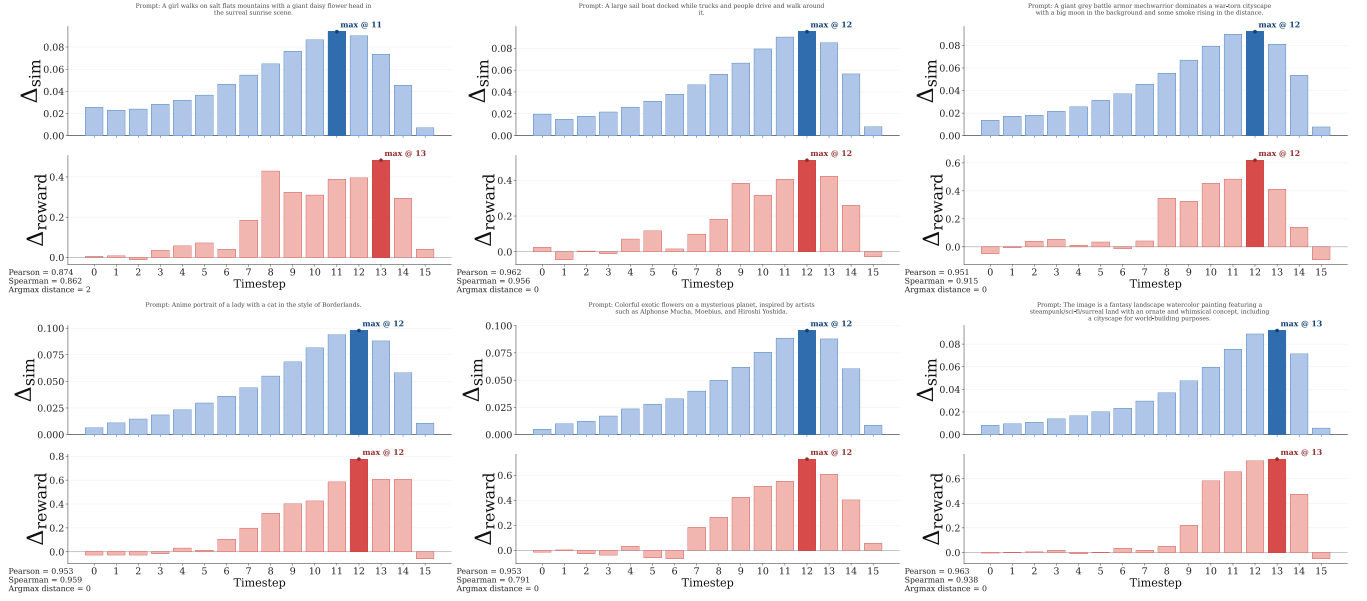


Figure 6: Qualitative evidence supporting the use of ΔS_t^i as a proxy for timestep contribution. The figure shows a clear correlation between ΔS_t^i and ΔR_t^i .

tracks the evolution of reward improvement along the denoising trajectory and effectively localizes the denoising steps that are most critical to the final reward gain, further supporting its use as an effective timestep-wise contribution proxy.

6.2 Exploration-Biased Objective Formulation

We briefly analyze the exploration bias introduced in Eq. (12)–(14). The trajectory score $q_i = \sum_t w_t^i \Delta S_t^i$ summarizes the weighted structural contribution of a sampled path across denoising steps. A larger $|q_i|$ indicates that the trajectory exhibits stronger step-wise alignment changes toward the final state, and therefore reflects a more distinctive and potentially informative generation process. Such trajectories deviate more noticeably from the group-average evolution pattern and are thus considered more worthwhile to explore.

To make this signal comparable across samples within a group, we normalize it using the group standard deviation, yielding $e_i = |q_i| / (\text{std}(\{q_j\}) + \epsilon)$. This standardization prevents the exploration strength from being dominated by absolute scale variations across prompts, ensuring that the bias reflects relative structural deviation rather than raw magnitude.

The exploration bias is activated only when the aggregated advantage is positive. This constraint ensures that we encourage directions that are already reward-consistent, rather than amplifying undesirable updates. The modulation term $\tanh(e_i)$ further keeps the exploration strength smoothly bounded, avoiding abrupt or unstable perturbations while preserving monotonic sensitivity to structural deviation.

With the introduction of λ_i , the original minimum-norm objective no longer purely favors the smallest aggregated advantage. Instead, it explicitly trades off between minimizing disagreement

and retaining larger positive advantages. As a result, objective mixtures associated with stronger reward signals receive increased preference, while the coefficient vector remains constrained on the probability simplex. When $\lambda_i = 0$, Eq. (13) reduces to the original minimum-norm objective in Eq. (11), and the solver degenerates to the conservative minimum-norm fusion. Therefore, the proposed exploration bias can be viewed as a smooth extension rather than a structural modification of the original formulation.

The multi-objective optimization in Eq. (13) can be equivalently reduced to a one-dimensional quadratic problem over the aggregated scalar $z = \mathbf{c}^T \mathbf{A}^i$:

$$\min_{z \in [s_{\min}, s_{\max}]} z^2 - \lambda_i z,$$

where $[s_{\min}, s_{\max}]$ denotes the feasible range induced by individual advantages. The objective $z^2 - \lambda_i z$ is a convex quadratic function in z , ensuring a unique global minimizer prior to projection. The solver in Algorithm 1 first computes the unconstrained minimizer $z^* = \lambda_i/2$, projects it onto this interval, and then recovers a coefficient vector via linear interpolation between neighboring objectives. This closed-form procedure is efficient, preserves the simplex constraint, and introduces only a smooth perturbation to the original minimum-norm formulation.

6.3 Algorithm Presentation.

To facilitate a clearer understanding of our method, we provide pseudocode-style frameworks of the proposed algorithms. Specifically, Algorithm 1 details the integration process among multiple reward components in the MOCA module, while Algorithm 2 illustrates the overall optimization pipeline of OTCA. These algorithmic presentations are intended to highlight the logical flow and design principles, rather than executable code.

Algorithm 1 Multi-Objective Credit Allocation (MOCA) Solver

Require: Advantages $\mathbf{A}^i = [A_1^i, \dots, A_K^i]$ for sample i ; exploration strength λ_i ; tolerance $\epsilon = 10^{-8}$

Ensure: Coefficient vector $\mathbf{c}^i \in \Delta^K$ (probability simplex)

- 1: // **Step 1: Determine feasible range of $z = \mathbf{c}^{i\top} \mathbf{A}^i$**
- 2: $s_{\min} \leftarrow \min_k A_k^i, \quad s_{\max} \leftarrow \max_k A_k^i$
- 3: **if** $s_{\max} - s_{\min} < \epsilon$ **then** ▷ Case 1: all advantages equal
- 4: $k^* \leftarrow \arg \max_k A_k^i$
- 5: **return** \mathbf{c}^i with $c_{k^*}^i = 1$ and $c_k^i = 0 \forall k \neq k^*$
- 6: **end if**
- 7: // **Step 2: Closed-form solution of $\min_z z^2 - \lambda_i z$, projected onto $[s_{\min}, s_{\max}]$**
- 8: $z^* \leftarrow \lambda_i / 2$
- 9: $\hat{z} \leftarrow \text{clip}(z^*, s_{\min}, s_{\max})$
- 10: **if** $\exists k$ s.t. $|A_k^i - \hat{z}| < \epsilon$ **then** ▷ Case 2: \hat{z} matches A_k^i exactly
- 11: **return** \mathbf{c}^i with $c_k^i = 1$ and $c_{k'}^i = 0 \forall k' \neq k$
- 12: **end if**
- 13: // **Step 3: Recover sparse \mathbf{c}^i via linear interpolation**
- 14: Sort indices so that $A_{(1)} \leq \dots \leq A_{(K)}$, with permutation π
- 15: $\mathbf{c}^i \leftarrow \mathbf{0}$
- 16: **for** $j = 1, \dots, K - 1$ **do**
- 17: **if** $A_{(j)} \leq \hat{z} \leq A_{(j+1)}$ **then** ▷ Case 3: bracket found
- 18: $c_{\pi(j)}^i \leftarrow \frac{A_{(j+1)} - \hat{z}}{A_{(j+1)} - A_{(j)}}$
- 19: $c_{\pi(j+1)}^i \leftarrow \frac{\hat{z} - A_{(j)}}{A_{(j+1)} - A_{(j)}}$
- 20: **break**
- 21: **end if**
- 22: **end for**
- 23: **return** \mathbf{c}^i

Algorithm 2 Objective-Aware Trajectory Credit Assignment (OTCA)

Require: Advantages \mathbf{A}^i ; latent trajectory $\{z_t^i\}_{t=1}^T$; final state z_{final}^i ; group statistics $\{q_j\}_{j=1}^G$; tolerance ϵ

Ensure: Timestep-specific effective advantages $\{\tilde{A}_t^i\}$

- 1: // **Step 1: Trajectory-Level Credit Decomposition (TCD)**
- 2: Compute similarity S_t^i between z_t^i and z_{final}^i
- 3: $\Delta S_t^i \leftarrow S_t^i - S_{t+1}^i$
- 4: $w_t^i \leftarrow \text{Normalize}(\max(0, \Delta S_t^i))$
- 5: // **Step 2: Multi-Objective Credit Allocation (MOCA)**
- 6: $q_i \leftarrow \sum_t w_t^i \Delta S_t^i$
- 7: $e_i \leftarrow \frac{|q_i|}{\text{std}_j(q_j) + \epsilon}$
- 8: $\lambda_i \leftarrow \frac{\max(0, \sum_k A_k^i)}{|\sum_k A_k^i| + \epsilon} \cdot \tanh(e_i)$
- 9: $\mathbf{c}^i \leftarrow \text{MOCASOLVER}(\mathbf{A}^i, \lambda_i)$ ▷ Algorithm 1
- 10: // **Step 3: Effective Advantage Construction**
- 11: $\tilde{A}_t^i \leftarrow w_t^i \cdot \mathbf{c}^{i\top} \mathbf{A}^i$
- 12: **return** $\{\tilde{A}_t^i\}$

6.4 Additional Qualitative Experiments

To further validate the effectiveness of OTCA, we provide additional qualitative results for both image and video generation. As shown in Fig. 7, Fig. 8, and Fig. 9, OTCA consistently produces more coherent and better-aligned outputs across diverse prompts and visual scenarios. These additional examples provide intuitive evidence that structured, timestep-aware reward credit assignment improves generation quality in both image and video domains.

6.4.1 Image Generation. Figure 7 presents additional qualitative results on image generation. Compared with the baselines, OTCA produces images with clearer subject structure, more faithful semantic correspondence to the prompt, and richer local details. These improvements are particularly evident in challenging cases that require coordinated optimization over multiple visual aspects, where coarse global supervision often leads to under-refined regions or inconsistent object appearance. Such results reflect the benefit of Trajectory-Level Credit Decomposition (TCD), which identifies the denoising steps that are most critical to the final output and enables timestep-specific optimization rather than uniformly broadcasting the same reward signal across the entire trajectory.

6.4.2 Video Generation. Figures 8 and 9 show additional qualitative results on video generation. OTCA yields videos with stronger semantic alignment, more coherent motion dynamics, and improved visual consistency across frames. In complex prompts involving multiple objectives, OTCA better preserves both appearance quality and temporal plausibility, while baseline methods are more prone to structural inconsistency or insufficient refinement. These gains highlight the importance of Multi-Objective Credit Allocation (MOCA), which adaptively balances heterogeneous reward signals in the advantage space, as well as TCD, which focuses optimization on the most reward-sensitive denoising stages. Together, these two components allow OTCA to refine both *when* to optimize and *what* to optimize, leading to more stable and effective visual GRPO training.

Overall, these additional qualitative examples further support our central claim that OTCA successfully transforms coarse global reward supervision into fine-grained, timestep-aware policy updates, resulting in stronger visual quality and more reliable alignment across both image and video generation.

6.5 Implementation Details

For TCD module, we use the weighting strategy with minimum weight $w_{\min} = 0.5$. The remaining timesteps are correspondingly upweighted to promote trajectory diversity and mitigate reward sparsity. Additionally, no timestep fraction is applied, which means all timesteps participate in optimization. For the exploratory MOCA module, we set $\epsilon = 10^{-6}$. We similarly rescale individual reward components to increase differentiation across reward terms and alleviate sparsity. For GRPO optimization, the importance ratio ρ_t^i is clipped at 10^{-4} . During sampling, we generate 12 samples per prompt for image generation and 8 for video generation. We set the gradient accumulation steps to 12 for image generation and 8 for video generation and use a learning rate of 1×10^{-5} . Same noise for generation is adopted.

Received 20 February 2007; revised 12 March 2009; accepted 5 June 2009

Alice is sticking her head out of a looking glass.



Cover of a Transformers Zine featured on Artstation.



A painting of a Victorian house titled "Fond Memories" by Mary Haley.



A highly detailed ukiyo-e style illustration of Dora the Explorer as a real girl.



A couple of horse that are eating some grass



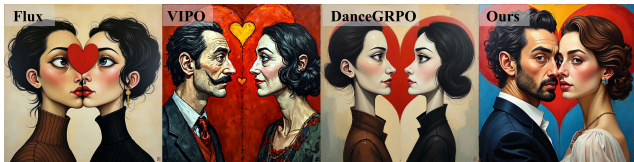
A girl is practicing fire magic surrounded by roaring flames.



An artwork from Dan Mumford collection featuring a mage invoking divine gods during a storm with lightnings.



A symmetrical male and female portrait, with a shared heart, created by artists Santiago Calatrava and Salvador Dali. An angel is protecting a man who is praying inside a gothic church.



A girl wearing a suit stands in the desert holding a giant carnation flower head, captured through the lens of surreal photography.



Hyperreal anthropomorphic ragdoll cat in cosplay outfits, illustrated with a big smile.



Fractal poster with an L-shaped tree design.



One sentence: An anthropomorphic lion in a highly detailed, colorful vector art portrait with smooth and clean curves.



A drawing of a magical forest created by an 8-year-old.



A large metal spoon sitting on top of a cup.



The image depicts a young female in ornate battle armor wearing a metallic helmet with long dark hair and symmetrical facial features.



An old drawing depicts a scuba diver and mermaid swimming underwater in a realistic style, with dramatic lighting and intense scenery.



Figure 7: More qualitative comparison of image generation. For each text prompt, the generated videos are shown from top to bottom using Flux1.0-dev, VIPO, DanceGRPO, and our proposed method, respectively.

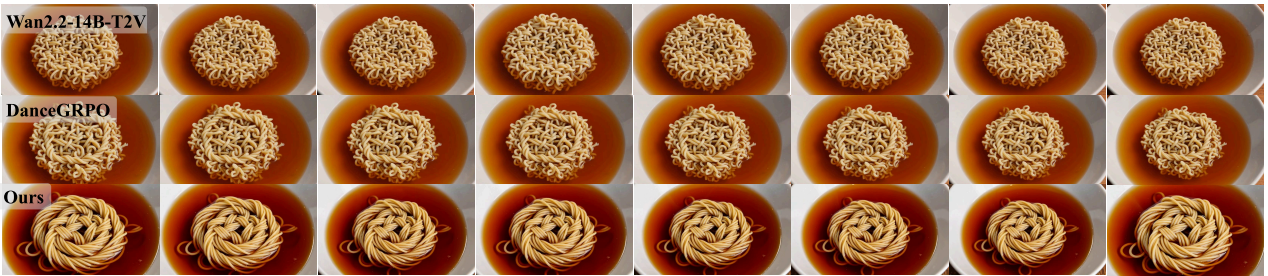
A 2D animation of a skateboarder doing a kickflip, the skateboard turning into a magic carpet mid-air



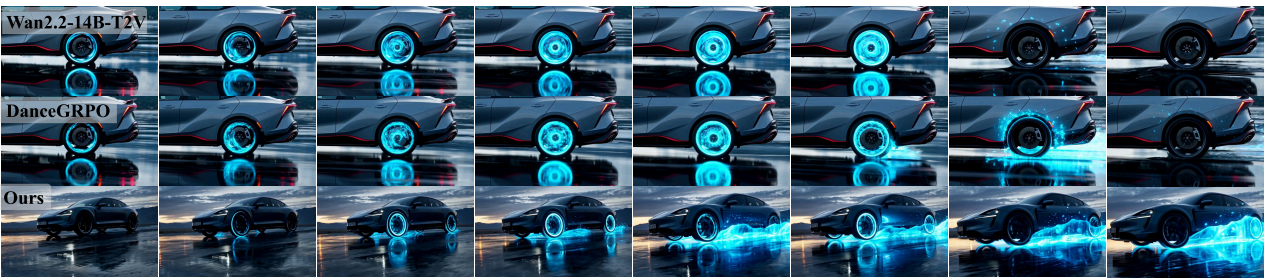
A block of dry ice in a pool of water, bubbling fiercely and generating a massive mushroom cloud of fog



A bowl of ramen where the noodles are braided together into a complex Celtic knot



A car driving on water, the wheels generating glowing blue waves that freeze instantly



A cat in a maid outfit violently sweeping dust bunnies that try to run away

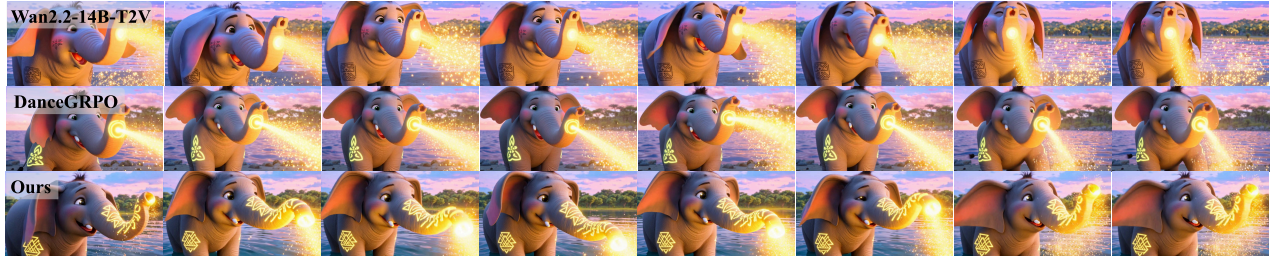


Figure 8: More qualitative comparison of video generation. For each text prompt, the generated videos are shown from top to bottom using Wan2.2, DanceGRPO, and our proposed method, respectively.

A child sweeping the floor, the dust gathering together to form a running dust-monster.



A cute baby elephant with glowing tribal tattoos spraying sparkling stardust out of its trunk instead of water



A dead, barren tree instantly erupting into a massive canopy of glowing pink cherry blossoms



A horse galloping on a treadmill, wearing high-tech glowing running shoes on all four hooves



A house made of books, the pages violently flapping in a strong wind without tearing



Figure 9: More qualitative comparison of video generation. For each text prompt, the generated videos are shown from top to bottom using Wan2.2, DanceGRPO, and our proposed method, respectively.